CONDENSED MATTER PHYSICS

Topological insulator metamaterial with giant circular photogalvanic effect

X. Sun[1,2]*, G. Adamo[1,2]*, M. Eginligil[2†], H. N. S. Krishnamoorthy[1,2], N. I. Zheludev[1,2,3], C. Soci[1,2‡]

One of the most notable manifestations of electronic properties of topological insulators is the dependence of the photocurrent direction on the helicity of circularly polarized optical excitation. The helicity-dependent photocurrents, underpinned by spin-momentum locking of surface Dirac electrons, are weak and easily overshadowed by bulk contributions. Here, we show that the chiral response can be enhanced by nanostructuring. The tight confinement of electromagnetic fields in the resonant nanostructure enhances the photoexcitation of spin-polarized surface states of topological insulator $Bi_{1.5}Sb_{0.5}Te_{1.8}Se_{1.2}$, leading to an 11-fold increase of the circular photogalvanic effect and a previously unobserved photocurrent dichroism ($\rho_{circ} = 0.87$) at room temperature. The control of spin transport in topological materials by structural design is a previously unrecognized ability of metamaterials that bridges the gap between nanophotonics and spin electronics, providing opportunities for developing polarization-sensitive photodetectors.

INTRODUCTION

Chirality, or the difference of an object from its mirror image, is a ubiquitous and fascinating phenomenon in nature. It manifests itself at a variety of scales and forms, from galaxies to nanotubes and from organic molecules to inorganic compounds. Detection of chirality at the molecular or atomic level is the key to fundamental sciences (e.g., chemistry, biology, and crystallography) and practical applications (e.g., food and pharmaceutical industry) yet very challenging. Detection of chirality relies on the interaction with electromagnetic fields, which is hindered by the large mismatch between the wavelength of light and the size of most molecules and crystalline unit cells, thereby resulting in nearly imperceptible twists of the light field over nanoscale dimensions.

In recent years, the chiral response of topological materials, such as topological insulators (*1*–*4*), Dirac/Weyl semimetals (*5*–*8*), and two-dimensional (2D) van der Waals heterostructures (*9*, *10*), underpinned by the peculiar quantum features of their electronic structures, have been the subject of intense investigation. For instance, the surfaces of 3D topological insulators support chiral spin currents, a net directional flow of spins in the absence of a net flow of charges. While the spin texture of surface electrons in topological insulators can be unraveled by scanning tunneling spectroscopy (*11*, *12*) or angular resolved photoemission spectroscopy (*1*, *13*, *14*), direct electrical or optical addressing of chiral surface states in this class of materials is hampered by the large contribution of the semiconducting bulk to the conductivity, induced by unintentional doping (*15*–*18*).

One of the most notable manifestations of the electronic chirality of topological insulator surface states is the dependence of their photocurrent on light helicity. Spin currents can be transformed into polarized net electrical currents when the system is optically driven out of equilibrium (*2*, *19*) by the helicity of light excitation: The absorption of circularly polarized light incident on the surface at oblique angles induces an unbalance between surface carriers of opposite spin at specific points in the *k*-space, thereby generating topological, spin-momentum–locked photocurrents.

Attempts to magnify helicity-dependent photocurrent (HDPC) in topological materials have relied on strategies to increase the inherent surface-to-bulk contribution, such as using Bi-chalcogenides with low intrinsic doping (*3*, *20*–*22*), reducing the crystal thickness to only a few quintuple layers (*23*), tuning the Fermi energy by electrical gating (*24*), or selectively exciting surface carriers below the bulk bandgap (*25*). More recently, research has broadened to Weyl semimetals, where the "chiral anomaly" (*6*, *7*, *26*), induced by unpaired Dirac cones, is expected to yield highly chiral photocurrents.

Designer metamaterials, with structural features comparable to the wavelength of light, provide an independent approach to devise optical properties on demand and enhance light-matter interaction (*27*). The creation and enhancement of optical chirality by metamaterials is particularly interesting and elaborate (*28*–*31*). For instance, patterning an achiral medium (e.g., a metal) with chiral, subwavelength shapes makes the resulting metamaterial intrinsically chiral. Similarly, the mutual orientation of a metamaterial, patterned with nonchiral structures, and the incident electromagnetic wave can lead to an extrinsically chiral response (*32*, *33*). Both forms of chirality can emerge in 2D and 3D metamaterial systems and lead to strong optical activity, circular dichroism, and asymmetric transmission.

Here, we provide a first demonstration of the use of artificial nanostructuring to enhance the chiral photogalvanic response of topological insulators. Thanks to the tight confinement of electromagnetic fields, resonant nonchiral metamaterials effectively enhance the photoexcitation of spin-polarized states, thereby increasing the unbalance between surface-state carriers with opposite spin helicity and overall resulting in a giant enhancement of the extrinsic chiral photocurrent response of a 3D topological insulator (TI), Bi1.5Sb0.5Te1.8Se1.2 (BSTS).

[1]Centre for Disruptive Photonic Technologies, TPI, SPMS, Nanyang Technological University, Singapore 637371, Singapore. [2]Division of Physics and Applied Physics, Nanyang Technological University, Singapore 637371, Singapore. [3]Optoelectronics Research Centre and Centre for Photonic Metamaterials, University of Southampton, Southampton SO17 1BJ, UK.
*These authors contributed equally to this work.
†Present address: Key Laboratory of Flexible Electronics (KLOFE) and Institute of Advanced Materials (IAM), Nanjing Tech University, 30 South Puzhu Road, Nanjing 211800, China.
‡Corresponding author. Email: csoci@ntu.edu.sg

RESULTS AND DISCUSSION

Helicity-dependent photocurrent

Surface carriers can be selectively excited in topological insulators by circularly polarized light directed at oblique incidence on the surface of the crystal, and the resulting current flow is determined by the spin-momentum locking of the carriers (Fig. 1). As the topological insulator crystal is intrinsically achiral (the surface states have equal number of carriers with opposite spin orientations), and the relevant spins lay in the surface plane of the crystal, photoexcitation at normal incidence does not generate any HDPC. However, spin-selective photoexcitation of surface-state carriers by obliquely incident light with a given helicity induces chirality (unbalance in the populations of surface state carriers with opposite spin orientations), akin to the extrinsic chirality described for metamaterials. This effect, known as the circular photogalvanic effect (CPGE) (*34*–*36*), is illustrated in Fig. 1A, where a light beam of defined handedness selectively promotes carriers of matching spin from surface to bulk conduction bands, thus leaving the surface bands asymmetrically depopulated in *k*-space: The excess surface carriers of opposite spin generate the net spin-polarized electrical current, j_a. The presence of a nanostructure on the surface of topological insulators, designed to have a resonant absorption at the wavelength of excitation, effectively increases the number of surface conduction carriers that are promoted to the bulk conduction bands (Fig. 1B), thus significantly enhancing the CPGE contribution to the photocurrent. Figure 1C shows the experimental arrangement to measure HDPC: Light is incident at a variable angle, θ, on the surface of the topological insulator crystal (*xy* plane), and the light polarization is changed continuously from linear to circular by rotating a quarter-wave plate, whose fast axis forms an angle, φ, with the polarization axis. Without any applied bias, an HDPC flows across the two gold contacts on the crystal surface.

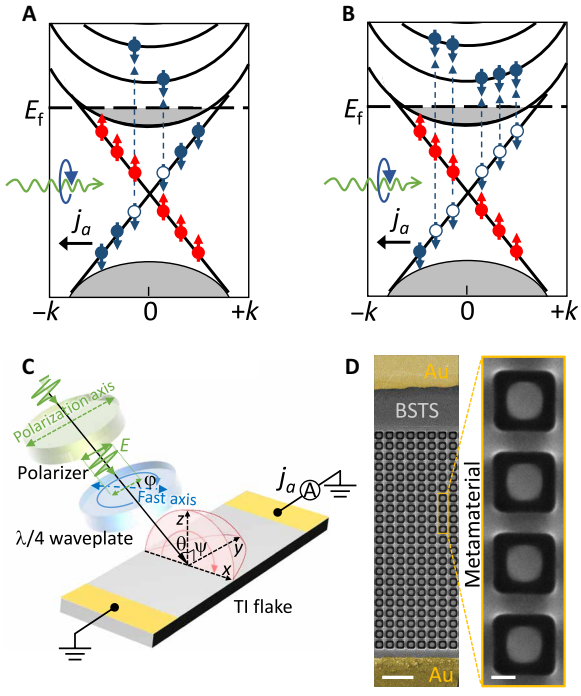

Fig. 1. HDPC in topological insulators and topological insulator metamaterials. (**A**) In an unstructured topological insulator (TI), Dirac electrons with spin coupled to a given circular polarization of incident light (blue) are promoted to higher bands in the *k*-space; the excess of spin-momentum–locked surface-state electrons with opposite spin (red) gives rise to an HDPC, j_a (circular photogalvanic effect). (**B**) In a TI metamaterial, a larger number of spin-polarized electrons are photoexcited upon resonant light absorption, enhancing the HDPC. (**C**) Schematic of the HDPC experimental setup, illustrating the mutual orientation of the electrodes on the TI device relative to the laser excitation beam at incidence angle θ and polarization defined by the angle of rotation φ of the quarter-wave plate. (**D**) SEM image of the square ring metamaterial carved between the Au electrodes on the surface of a TI flake. Scale bars, 1 μm on the left and 100 nm on the right.

Optical absorption and metamaterial design

To assess the enhancement of chirality exclusive to topological surface spin currents, we chose a metamaterial design that does not introduce optical chirality, neither intrinsic nor extrinsic (*37*). The metamaterial unit cells consist of square rings of ~200-nm lateral size and ~100-nm ring width, arranged on a square lattice of ~335-nm period. Such pattern was carved by focused ion beam (FIB) milling between two gold electrodes deposited on a ~250-nm-thin BSTS flake, as shown in the scanning electron microscopy (SEM) images in Fig. 1D.

The metamaterial was designed to resonantly increase the optical absorption of the unstructured BSTS flake at the excitation wavelength, λ = 532 nm, at both normal (θ = 0°) and oblique (θ = 45°) incidence (Fig. 2). The experimental and numerically simulated spectra of the BSTS metamaterial (Fig. 2A, right) show a resonant increase in optical absorption with respect to the case of unstructured BSTS (Fig. 2A, left). Following from the design symmetry, the metamaterial geometry does not induce any helicity dependence to the bulk response of the BSTS flake, as confirmed by the maps of electric field intensity for circularly polarized light of opposite handedness (Fig. 2, B and C).

Control of CPGE in topological insulator by the metamaterials

We measured HDPC under nearly uniform illumination (laser beam diameter of ~200 μm, much larger than the BSTS device size of ~10 μm), with no applied bias (Fig. 3). The residual un-uniformity of illumination results in thermal gradient that induces polarization-independent photothermoelectric currents, which contribute to the photocurrent background. This component of the current is sensitive to the position of the excitation beam on the sample (*3*).

To measure a clearly distinguishable photocurrent signal, we adjusted the laser beam position on the BSTS flake and BSTS metamaterials to obtain the maximum total photocurrent, i.e., we maximized the thermoelectric photocurrent offset (see section S1 and figs. S1A and S2). Contributions of surface carriers to the photocurrent, seen in HDPC, are allowed only at oblique illumination (*2*), as illustrated in the top section of Fig. 3A. We measured the photocurrent, j_a, shining the laser at θ = − 45° and going through a full rotation cycle of its polarization angle, φ, from 0° to 360°. This induces a continuous change of the incident polarization, from linear (φ = 0°, 90°) to circular of right (φ = 45°) and left (φ = 135°) handedness, with 180° period.

The bottom panel of Fig. 3A shows the photocurrent, j_a, measured in an unstructured BSTS flake (black-filled squares). The current has the characteristic polarization-dependent behavior observed in other Bi-chalcogenide topological insulators (*3*, *20*, *24*) and other 2D material systems [i.e., quantum wells (*34*, *35*), transition metal dichalcogenide (*8*, *38*, *39*), and Weyl semimetals (*6*, *7*, *26*)]. It

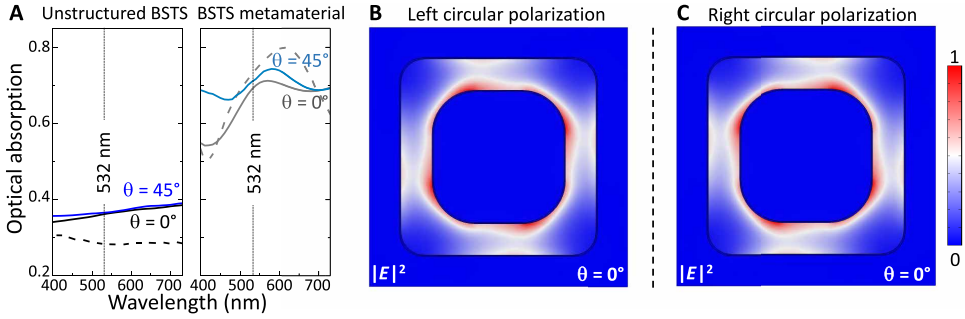

Fig. 2. Optical absorption enhancement in BSTS achiral metamaterial. (**A**) Measured (dashed lines) and simulated (continuous lines) optical absorption of an unstructured BSTS flake and a nanostructured BSTS metamaterial (experimental data were collected with unpolarized light at normal incidence and numerical aperture = 0.7, while simulations correspond to circularly polarized light incident at θ = 0° and θ = 45°); at λ = 532 nm, the absorption of the BSTS metamaterial is ~0.7, twice that of the unstructured BSTS flake (~0.35). (**B** and **C**) Maps of the electric field intensity, $|E|^2$, at 10 nm below the top surface of the metamaterial unit cell at normal incidence, for left (LCP) and right (RCP) circular polarization, respectively.

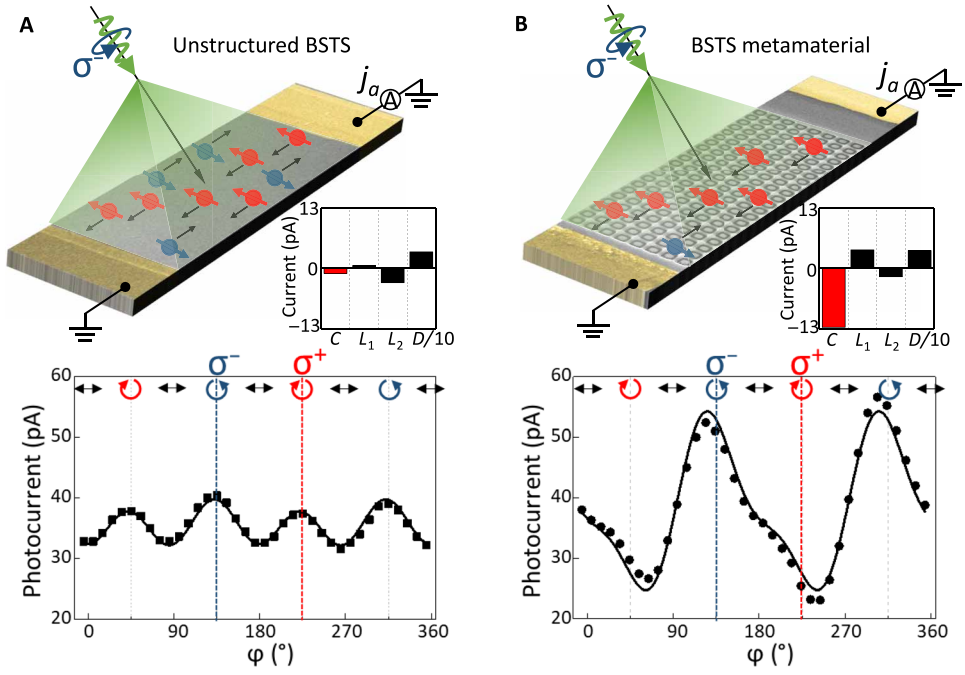

Fig. 3. Multifold increase of CPGE in BSTS topological insulator by metamaterials. (**A**) (top) Schematic of HDPC in an unstructured BSTS flake; (bottom) experimental photocurrent measured on an unstructured BSTS flake, at room temperature, and fitting with Eq. 1, showing the expected 4φ dependence and a small 2φ asymmetry between right (σ^+) and left (σ^-) circularly polarized illumination; (inset) fitting coefficient C, L_1, L_2, and D, indicating a predominance of bulk photon-drag contribution, L_2, in the photocurrent modulation. (**B**) (top) Schematic of light HDPC in a nanostructured BSTS metamaterial; (bottom) experimental photocurrent measured on a nanostructured BSTS metamaterial, at room temperature, and fitting with Eq. 1, showing how the metamaterial induces a 2φ dependence that indicates that the sample responds almost exclusively to right (σ^+) and left (σ^-) circularly polarized illumination; (inset) fitting coefficient C, L_1, L_2, and D, indicating a predominance of CPGE, C, in the photocurrent modulation.

composes of four components, expressed by the phenomenological equation (*3*, *35*)

$$j_a = C \sin 2\varphi + L_1 \sin 4\varphi + L_2 \cos 4\varphi + D \quad (1)$$

The coefficients D and L_2 are associated to photocurrent contributions from the semiconducting bulk. Specifically, D is related to the polarization-independent photothermoelectric background current, which sets the overall directional current flow, while L_2 to the photon drag effect, which results from linear momentum transfer of the incident photons to the excited carriers. Conversely, the coefficients L_1 and C quantify photocurrent contributions from surface carriers. Such currents, driven by linear and circular polarization of the incident light, originate from the linear and circular photogalvanic effects, respectively. The dependence of the photocurrent on helicity is seen in the small asymmetry between the peaks corresponding to photoexcitation by light of opposite handedness (σ^+ and σ^- in the bottom panel of Fig. 3A). The relative contribution of each surface

and bulk component to the total photocurrent is shown in the bar plot of the coefficients of Eq. 1 (inset of Fig. 3A). While surface contributions to the photocurrent are discernible even at room temperature in the unstructured BSTS samples [thanks to the large surface-to-bulk conductivity known for this particular stoichiometry (*22*, *40*–*42*)], their dependence on light helicity is overshadowed by bulk components (C/D = 0.03) and too small for any practical device or application.

The very same BSTS flake, patterned with square ring metamaterial array, behaves markedly differently. The resonant metamaterial structure induces much larger asymmetry in the population of surface conducting bands, increasing the net spin current (top schematic in Fig. 3B). The effect is so strong that the measured photocurrent (black-filled circles in bottom panel of Fig. 3B) has a distinct 2φ evolution as function of polarization, irrespective of the contribution of linearly polarized components (*43*). The effect is even more apparent when comparing the coefficients of Eq. 1 (inset of Fig. 3B), where, now, C is far higher than the linear coefficients, L_1 and L_2, and its value accounts for a significant fraction of the photocurrent (C/D = 0.33). Table 1 summarizes the fitting coefficients of photocurrents, j_a, for both unstructured and nanostructured BSTS, at and off normal incidence. The photocurrent circular dichroism induced by spin-polarized surface states can be defined as (*35*)

$$\rho_{circ} = \frac{|I_{\sigma^+} - I_{\sigma^-}|}{|I_{\sigma^+} + I_{\sigma^-}|} \quad (2)$$

where $I_{\sigma+}$ and $-I_{\sigma-}$ are, respectively, the values of photocurrents under left and right circularly polarized optical excitation, excluding the spin-insensitive component D (*44*). A threefold increase of the degree of spin polarization of unstructured BSTS (ρ_{circ} = 0.26) is seen in the BSTS metamaterial (ρ_{circ} = 0.87), an unprecedented degree of spin polarization approaching unity even at room temperature in nonmagnetic materials (*44*–*47*). Additional validation of the functional dependence of the HDPC on incidence angle θ is shown in the Supplementary Materials (section S2 and figs. S3 and S4). Notably, the surface nature of HDPC in BSTS was also confirmed, repeating the experiments on a trivial chalcogenide insulator of the same family, Bi_2S_3, where we measured only bulk currents (section S3 and figs. S5 and S6).

For a given angle of incidence, the j_a coefficients of both, unstructured and nanostructured BSTS, have equal sign, which reverses at mirror angles of incidence (Table 1 and fig. S3). This proves that the metamaterial does not introduce chirality (*37*, *48*) but rather enhances the extrinsic chirality of the BSTS surface layer.

Electromagnetic modeling

In the following, we describe the photocurrent behavior of spin-transport metamaterials by electromagnetic modeling. The generated photocurrent is directly proportional to the optical absorption, carrier density, mobility, and lifetime of the topological insulator. Thus, under the assumption that the optical absorption of the BSTS metamaterial increases upon nanostructuring, while the remaining transport parameters remain unaltered, carrier anisotropy can be mapped to an anisotropic optical model of the BSTS topological insulator crystal (Fig. 4). Here, we describe the unstructured BSTS crystal by its isotropic relative permittivity, ε_r [experimentally determined by ellipsometric measurements (*49*)], modified by ad hoc off-diagonal terms of the permittivity tensor to mimic the effective optical chirality induced by the in-plane spin of Dirac surface electrons. We performed full-wave electromagnetic simulations for both unstructured and nanostructured BSTS, replicating the sample illumination conditions used in the experiments (λ = 532 nm; θ = 0, ±45°; φ = 0° to 360°) and integrated the electric field intensity within the top 3 nm (*50*) to evaluate the optical absorption at the surface of the topological insulator.

The electromagnetic modeling (Fig. 4B) is in excellent agreement with the experimental HDPC result (Fig. 4A), corroborating the link between anisotropic optical absorption at the BSTS surface and selective spin-photocurrent generation. The normalized polar plots in Fig. 4 (A and B) provide an immediate visualization of the prominence of linear components (four lobes) versus circular components (two lobes) in unstructured and nanostructured BSTS. While at normal incidence, the BSTS metamaterial does not produce any notable effect; at oblique incidence, it filters out linear components, distilling the response to circularly polarized light illumination and leading to a giant enhancement of the chiral photocurrent. The degree of chirality predicted by the simulations, according to the same Eq. 2, is ρ_{circ} = 0.18 for the unstructured BSTS and ρ_{circ} = 0.89 for the BSTS metamaterial, in excellent agreement with the values obtained experimentally (refer also to section S4 and fig. S7). Furthermore, in both experiments and simulations, illumination from mirror directions of incidence (with respect to the normal) yields opposite phases, just as expected for extrinsic chirality.

To conclude, the hitherto unrecognized ability of metamaterials to control surface transport in topological insulator by structural design provides a powerful toolbox to bridge the gap between nanophotonics and spin electronics. We have shown that resonant nanostructures can be used to induce giant enhancement of the extrinsic chiral photocurrent response of a topological insulator. We argue that this approach could be used to exert control over spin-transport properties of other classes of quantum and topological materials

Table 1. Fitting coefficients of the HDPC in unstructured BSTS flake and nanostructured BSTS metamaterials.

θ (°)	BSTS flake	C (pA)	L_1 (pA)	L_2 (pA)	D (pA)
−45	Unstructured	−1.1 ± 0.1	0.6 ± 0.1	−3.1 ± 0.1	35.4 ± 0.1
	Nanostructured	−12.7 ± 0.3	4 ± 0.3	−1.8 ± 0.3	38.3 ± 0.3
0	Unstructured	0.05 ± 0.05	−0.002 ± 0.05	0.09 ± 0.05	8.5 ± 0.05
	Nanostructured	−0.2 ± 0.04	−0.2 ± 0.04	0.04 ± 0.04	11.4 ± 0.04
45	Unstructured	1.0 ± 0.1	0.32 ± 0.1	−3.2 ± 0.1	35.1 ± 0.1
	Nanostructured	11 ± 0.4	−0.9 ± 0.4	−3 ± 0.4	41.8 ± 0.4

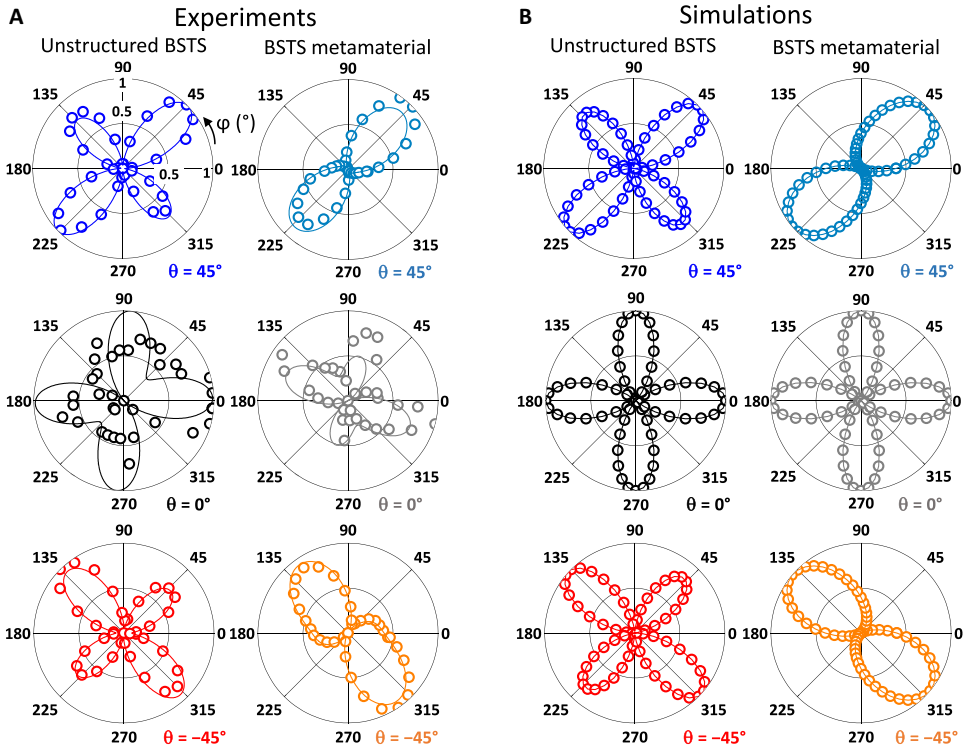

Fig. 4. Distillation of CPGE in BSTS topological insulator flakes by nanostructured metamaterials. (**A**) Normalized polar plots of HDPC for an unstructured BSTS flake (left column) and a nanostructured BSTS metamaterial (right column) at three different angles of incidence, θ = 45° (top row), θ = 0° (center row), and θ = −45° (bottom row); at θ = 0°, mostly L_2 contributes to the modulation of the photocurrent; at θ = 45° and θ = −45, the HDPC patterns of the unstructured BSTS flake and the BSTS metamaterial are distinctively different: The metamaterial distils the *C* term contribution to the photocurrent modulation, with respect to the unstructured BSTS flake, where L_1, L_2, and *C* have comparable amplitudes. (**B**) Simulated $|E|^2$ in both unstructured 250-nm BSTS film (left column) and nanostructured BSTS metamaterial (right column) at three different angles of incidence, θ = 45° (top row), θ = 0° (center row), and θ = −45° (bottom row), with artificially increased chirality of the optical permittivity, ε_r, of the BSTS; the distinct behavior observed in the unstructured BSTS and the BSTS metamaterial matches remarkably well with the measured photocurrent, indicating how the chirality of the surface carriers and the increased absorption given by the metamaterial result in a giant increase of the CPGE; the $|E|^2$ is integrated in a 3-nm-thin slab at the surface of the film. To better visualize the polarization (φ) dependence of both experimental data and numerical model, we subtract the polarization independent background from each curve and normalize them.

(e.g., Weyl semimetals and van der Waals heterostructures) and to find application in integrated spin-polarized photodetectors that are in great demand for ultrasensitive chiral molecular sensing and quantum optospintronic devices, where polarization and entanglement could be transferred from photons to electron spins.

MATERIALS AND METHODS

Device fabrication

$Bi_{1.5}Sb_{0.5}Te_{1.8}Se_{1.2}$ single crystals were grown using a modified Bridgeman method. This particular BSTS stoichiometry yields large surface-to-volume conductivity, so that transport in nanometric thin flakes is surface dominated (*22*). BSTS flakes were mechanically exfoliated and transferred from the bulk crystals onto a SiO_2 (285 nm)/*P*-Si substrates. Electrical contacts (Cr/Au 5/50 nm) for photocurrent measurements were created on the devices by electron beam lithography and thermal evaporation. Square ring metamaterials were carved on the BSTS flake between the contacts by FIB milling. All fabrication steps were performed minimizing the exposure of BSTS to the electron and ion beams. SEM images were acquired after photocurrent measurements.

HDPC measurement

Photocurrent measurements were performed at room temperature, illuminating the devices with continuous wave laser (λ = 532 nm) and with no applied bias. The linearly polarized laser beam was modulated at a frequency of 137 Hz by an optical chopper before passing through a λ/4 retarder and focused to a spot size of ~200-μm diameter between the electrodes. The experimental setup allowed to continuously vary the polarization of incident light from linear (s-polarized) to circular [right circular polarization (RCP) and left circular polarization (LCP)] by rotating the λ/4 wave plate. The incident light polarization was calibrated by a polarimeter. The photocurrent was measured with a lock-in amplifier referenced to the light modulation frequency. In all samples, the photocurrent was found to be linearly dependent on excitation intensity (refer to fig. S1B). All the measurements were performed at a constant illumination intensity of 10 W cm^{-2}.

Electromagnetic simulations

3D electromagnetic simulations were performed using COMSOL Multiphysics. The square ring metamaterial dimensions were derived from the SEM images. The relative permittivity of BSTS, ε_{r_ell} (isotropic), was experimentally obtained by ellipsometry (see section S5 and fig. S8). The simulations were built to match the experimental arrangement shown in Fig. 1C: The square rings were laying on the *xy* plane and extruded through the *z* direction; the direction of incidence of the electromagnetic wave was laying in the *xz* plane, with an elevation angle, θ (0°, ±45°), with respect to the *z* axis; the

incident wave polarization was obtained by introducing a φ dependence to the two orthogonal components (h, v) of the electric field with a π/2 phase retardation: $h = (1 - i)*[\sin(\varphi)*\cos(\varphi)]$, $v = \sin(\varphi)^2 + i*\cos(\varphi)^2$. The simulations of the optical absorption (Fig. 2A) of the square ring BSTS metamaterials were performed using the isotropic, ellipsometrically measured ε_{r_ell}. The simulations of $|E|^2$ (Fig. 4B and fig. S7) were performed, introducing an anisotropic response along the x direction, by assigning nonzero values to the off-diagonal terms of the permittivity tensor. The diagonal terms of the permittivity tensor were defined as $\varepsilon_{xx,yy,zz} = \varepsilon_{r\_ell}$, while the off-diagonal terms were defined as $\varepsilon_{yz,zy} = \pm i*\chi$, with $v = 0.36*\varepsilon_{r\_ell}$. The electric field intensity $|E|^2$ plotted in the graphs of Fig. 4B and fig. S7 was obtained by performing a volume integration of $|E|^2$ within a 3-nm-thin slab from the surface. The anisotropic response along the x direction was introduced by assigning nonzero values to the off-diagonal terms of the permittivity tensor, $\varepsilon_{r(yz,zy)} = \pm j*\varepsilon_{r(xx,yy,zz)}$. The incident wave polarization rotation, reproducing the experimental arrangement of polarizer and quarter-wave plate, was obtained by introducing a φ dependence to both s and p components of the electric field with a π/2 phase retardation between the two. The electric field intensity plotted in the graphs was obtained by integrating the $|E|^2$ within a 3-nm-thin slab from the surface.

SUPPLEMENTARY MATERIALS

Supplementary material for this article is available at http://advances.sciencemag.org/cgi/content/full/7/14/eabe5748/DC1

REFERENCES AND NOTES

1. D. Hsieh, Y. Xia, D. Qian, L. Wray, J. H. Dil, F. Meier, J. Osterwalder, L. Patthey, J. G. Checkelsky, N. P. Ong, A. V. Fedorov, H. Lin, A. Bansil, D. Grauer, Y. S. Hor, R. J. Cava, M. Z. Hasan, A tunable topological insulator in the spin helical Dirac transport regime. *Nature* **460**, 1101–1105 (2009).
2. P. Hosur, Circular photogalvanic effect on topological insulator surfaces: Berry-curvature-dependent response. *Phys. Rev. B* **83**, 035309 (2011).
3. J. W. McIver, D. Hsieh, H. Steinberg, P. Jarillo-Herrero, N. Gedik, Control over topological insulator photocurrents with light polarization. *Nat. Nanotechnol.* **7**, 96–100 (2012).
4. A. Junck, G. Refael, F. von Oppen, Photocurrent response of topological insulator surface states. *Phys. Rev. B* **88**, 075144 (2013).
5. C.-K. Chan, N. H. Lindner, G. Refael, P. A. Lee, Photocurrents in Weyl semimetals. *Phys. Rev. B* **95**, 041104 (2017).
6. Q. Ma, S.-Y. Xu, C.-K. Chan, C.-L. Zhang, G. Chang, Y. Lin, W. Xie, T. Palacios, H. Lin, S. Jia, P. A. Lee, P. Jarillo-Herrero, N. Gedik, Direct optical detection of Weyl fermion chirality in a topological semimetal. *Nat. Phys.* **13**, 842–847 (2017).
7. Z. Ji, G. Liu, Z. Addison, W. Liu, P. Yu, H. Gao, Z. Liu, A. M. Rappe, C. L. Kane, E. J. Mele, R. Agarwal, Spatially dispersive circular photogalvanic effect in a Weyl semimetal. *Nat. Mater.* **18**, 955–962 (2019).
8. S.-Y. Xu, Q. Ma, Y. Gao, A. Kogar, A. Zong, A. M. Mier Valdivia, T. H. Dinh, S.-M. Huang, B. Singh, C.-H. Hsu, T.-R. Chang, J. P. C. Ruff, K. Watanabe, T. Taniguchi, H. Lin, G. Karapetrov, D. Xiao, P. Jarillo-Herrero, N. Gedik, Spontaneous gyrotropic electronic order in a transition-metal dichalcogenide. *Nature* **578**, 545–549 (2020).
9. J. R. Wallbank, D. Ghazaryan, A. Misra, Y. Cao, J. S. Tu, B. A. Piot, M. Potemski, S. Pezzini, S. Wiedmann, U. Zeitler, T. L. M. Lane, S. V. Morozov, M. T. Greenaway, L. Eaves, A. K. Geim, V. I. Fal, ko, K. S. Novoselov, A. Mishchenko, Tuning the valley and chiral quantum state of Dirac electrons in van der Waals heterostructures. *Science* **353**, 575–579 (2016).
10. J. C. W. Song, N. M. Gabor, Electron quantum metamaterials in van der Waals heterostructures. *Nat. Nanotechnol.* **13**, 986–993 (2018).
11. T. Zhang, P. Cheng, X. Chen, J.-F. Jia, X. Ma, K. He, L. Wang, H. Zhang, X. Dai, Z. Fang, X. Xie, Q.-K. Xue, Experimental demonstration of topological surface states protected by time-reversal symmetry. *Phys. Rev. Lett.* **103**, 266803 (2009).
12. Z. Alpichshev, J. G. Analytis, J. H. Chu, I. R. Fisher, Y. L. Chen, Z. X. Shen, A. Fang, A. Kapitulnik, STM imaging of electronic waves on the surface of Bi_2Te_3: Topologically protected surface states and hexagonal warping effects. *Phys. Rev. Lett.* **104**, 016401 (2010).
13. H. Soifer, A. Gauthier, A. F. Kemper, C. R. Rotundu, S. L. Yang, H. Xiong, D. Lu, M. Hashimoto, P. S. Kirchmann, J. A. Sobota, Z. X. Shen, Band-resolved imaging of photocurrent in a topological insulator. *Phys. Rev. Lett.* **122**, 167401 (2019).
14. D. Hsieh, Y. Xia, L. Wray, D. Qian, A. Pal, J. H. Dil, J. Osterwalder, F. Meier, G. Bihlmayer, C. L. Kane, Y. S. Hor, R. J. Cava, M. Z. Hasan, Observation of unconventional quantum spin textures in topological insulators. *Science* **323**, 919–922 (2009).
15. D. Hsieh, F. Mahmood, J. W. McIver, D. R. Gardner, Y. S. Lee, N. Gedik, Selective probing of photoinduced charge and spin dynamics in the bulk and surface of a topological insulator. *Phys. Rev. Lett.* **107**, 077401 (2011).
16. D. Panna, R. Marjieh, E. Sabag, L. Rybak, A. Ribak, A. Kanigel, A. Hayat, Linear-optical access to topological insulator surface states. *Appl. Phys. Lett.* **110**, 212103 (2017).
17. P. Seifert, K. Vaklinova, K. Kern, M. Burghard, A. Holleitner, Surface state-dominated photoconduction and THz generation in topological Bi_2Te_2Se nanowires. *Nano Lett.* **17**, 973–979 (2017).
18. Y. Shao, K. W. Post, J.-S. Wu, S. Dai, A. J. Frenzel, A. R. Richardella, J. S. Lee, N. Samarth, M. M. Fogler, A. V. Balatsky, D. E. Kharzeev, D. N. Basov, Faraday rotation due to surface states in the topological insulator $(Bi_{1-x}Sb_x)_2Te_3$. *Nano Lett.* **17**, 980–984 (2017).
19. S. Raghu, S. B. Chung, X.-L. Qi, S.-C. Zhang, Collective modes of a helical liquid. *Phys. Rev. Lett.* **104**, 116401 (2010).
20. Y. Q. Huang, Y. X. Song, S. M. Wang, I. A. Buyanova, W. M. Chen, Spin injection and helicity control of surface spin photocurrent in a three dimensional topological insulator. *Nat. Commun.* **8**, 15401 (2017).
21. K. N. Okada, N. Ogawa, R. Yoshimi, A. Tsukazaki, K. S. Takahashi, M. Kawasaki, Y. Tokura, Enhanced photogalvanic current in topological insulators via Fermi energy tuning. *Phys. Rev. B* **93**, 081403 (2016).
22. B. Xia, P. Ren, A. Sulaev, P. Liu, S.-Q. Shen, L. Wang, Indications of surface-dominated transport in single crystalline nanoflake devices of topological insulator $Bi_{1.5}Sb_{0.5}Te_{1.8}Se_{1.2}$. *Phys. Rev. B* **87**, 085442 (2013).
23. J. Yu, K. Zhu, X. Zeng, L. Chen, Y. Chen, Y. Liu, C. Yin, S. Cheng, Y. Lai, J. Huang, K. He, Q. Xue, Helicity-dependent photocurrent of the top and bottom Dirac surface states of epitaxial thin films of three-dimensional topological insulators Sb_2Te_3. *Phys. Rev. B* **100**, 235108 (2019).
24. Y. Pan, Q.-Z. Wang, A. L. Yeats, T. Pillsbury, T. C. Flanagan, A. Richardella, H. Zhang, D. D. Awschalom, C.-X. Liu, N. Samarth, Helicity dependent photocurrent in electrically gated $(Bi_{1-x}Sb_x)_2Te_3$ thin films. *Nat. Commun.* **8**, 1037 (2017).
25. K. Kuroda, J. Reimann, J. Güdde, U. Höfer, Generation of transient photocurrents in the topological surface state of Sb_2Te_3 by direct optical excitation with midinfrared pulses. *Phys. Rev. Lett.* **116**, 076801 (2016).
26. F. de Juan, A. G. Grushin, T. Morimoto, J. E. Moore, Quantized circular photogalvanic effect in Weyl semimetals. *Nat. Commun.* **8**, 15995 (2017).
27. M. I. Stockman, K. Kneipp, S. I. Bozhevolnyi, S. Saha, A. Dutta, J. Ndukaife, N. Kinsey, H. Reddy, U. Guler, V. M. Shalaev, A. Boltasseva, B. Gholipour, H. N. S. Krishnamoorthy, K. F. MacDonald, C. Soci, N. I. Zheludev, V. Savinov, R. Singh, P. Groß, C. Lienau, M. Vadai, M. L. Solomon, D. R. Barton, M. Lawrence, J. A. Dionne, S. V. Boriskina, R. Esteban, J. Aizpurua, X. Zhang, S. Yang, D. Wang, W. Wang, T. W. Odom, N. Accanto, P. M. de Roque, I. M. Hancu, L. Piatkowski, N. F. van Hulst, M. F. Kling, Roadmap on plasmonics. *J. Opt.* **20**, 043001 (2018).
28. A. V. Rogacheva, V. A. Fedotov, A. S. Schwanecke, N. I. Zheludev, Giant gyrotropy due to electromagnetic-field coupling in a bilayered chiral structure. *Phys. Rev. Lett.* **97**, 177401 (2006).
29. N. Liu, H. Liu, S. Zhu, H. Giessen, Stereometamaterials. *Nat. Photonics* **3**, 157–162 (2009).
30. Y. Luo, C. Chi, M. Jiang, R. Li, S. Zu, Y. Li, Z. Fang, Plasmonic chiral nanostructures: Chiroptical effects and applications. *Adv. Opt. Mater.* **5**, 1700040 (2017).
31. M. Kadic, G. W. Milton, M. van Hecke, M. Wegener, 3D metamaterials. *Nat. Rev. Phys.* **1**, 198–210 (2019).
32. E. Plum, X. X. Liu, V. A. Fedotov, Y. Chen, D. P. Tsai, N. I. Zheludev, Metamaterials: Optical activity without chirality. *Phys. Rev. Lett.* **102**, 113902 (2009).
33. M. Ren, E. Plum, J. Xu, N. I. Zheludev, Giant nonlinear optical activity in a plasmonic metamaterial. *Nat. Commun.* **3**, 833 (2012).
34. S. D. Ganichev, E. L. Ivchenko, S. N. Danilov, J. Eroms, W. Wegscheider, D. Weiss, W. Prettl, Conversion of spin into directed electric current in quantum wells. *Phys. Rev. Lett.* **86**, 4358–4361 (2001).
35. S. D. Ganichev, W. Prettl, Spin photocurrents in quantum wells. *J. Phys. Condens. Matter* **15**, R935–R983 (2003).
36. S. D. Ganichev, J. Kiermaier, W. Weber, S. N. Danilov, D. Schuh, C. Gerl, W. Wegscheider, W. Prettl, D. Bougeard, G. Abstreiter, Subnanosecond ellipticity detector for laser radiation. *Appl. Phys. Lett.* **91**, 091101 (2007).
37. E. Plum, V. A. Fedotov, N. I. Zheludev, Extrinsic electromagnetic chirality in metamaterials. *J. Opt.* **11**, 074009 (2009).

38. H. Yuan, X. Wang, B. Lian, H. Zhang, X. Fang, B. Shen, G. Xu, Y. Xu, S.-C. Zhang, H. Y. Hwang, Y. Cui, Generation and electric control of spin–valley-coupled circular photogalvanic current in WSe_2. *Nat. Nanotechnol.* **9**, 851–857 (2014).
39. M. Eginligil, B. Cao, Z. Wang, X. Shen, C. Cong, J. Shang, C. Soci, T. Yu, Dichroic spin–valley photocurrent in monolayer molybdenum disulphide. *Nat. Commun.* **6**, 7636 (2015).
40. Z. Ren, A. A. Taskin, S. Sasaki, K. Segawa, Y. Ando, Optimizing $Bi_{2-x}Sb_xTe_{3-y}Se_y$ solid solutions to approach the intrinsic topological insulator regime. *Phys. Rev. B* **84**, 165311 (2011).
41. T. Arakane, T. Sato, S. Souma, K. Kosaka, K. Nakayama, M. Komatsu, T. Takahashi, Z. Ren, K. Segawa, Y. Ando, Tunable Dirac cone in the topological insulator $Bi_{2-x}Sb_xTe_{3-y}Se_y$. *Nat. Commun.* **3**, 636 (2012).
42. J. Yin, H. N. S. Krishnamoorthy, G. Adamo, A. M. Dubrovkin, Y. Chong, N. I. Zheludev, C. Soci, Plasmonics of topological insulators at optical frequencies. *NPG Asia Mater.* **9**, e425 (2017).
43. C. Kastl, C. Karnetzky, H. Karl, A. W. Holleitner, Ultrafast helicity control of surface currents in topological insulators with near-unity fidelity. *Nat. Commun.* **6**, 6617 (2015).
44. S. Cha, M. Noh, J. Kim, J. Son, H. Bae, D. Lee, H. Kim, J. Lee, H.-S. Shin, S. Sim, S. Yang, S. Lee, W. Shim, C.-H. Lee, M.-H. Jo, J. S. Kim, D. Kim, H. Choi, Generation, transport and detection of valley-locked spin photocurrent in WSe_2–graphene–Bi_2Se_3 heterostructures. *Nat. Nanotechnol.* **13**, 910–914 (2018).
45. O. V. Yazyev, J. E. Moore, S. G. Louie, Spin polarization and transport of surface states in the topological insulators Bi_2Se_3 and Bi_2Te_3 from first principles. *Phys. Rev. Lett.* **105**, 266806 (2010).
46. V. L. Korenev, I. A. Akimov, S. V. Zaitsev, V. F. Sapega, L. Langer, D. R. Yakovlev, Y. A. Danilov, M. Bayer, Dynamic spin polarization by orientation-dependent separation in a ferromagnet–semiconductor hybrid. *Nat. Commun.* **3**, 959 (2012).
47. J. Sánchez-Barriga, A. Varykhalov, J. Braun, S. Y. Xu, N. Alidoust, O. Kornilov, J. Minár, K. Hummer, G. Springholz, G. Bauer, R. Schumann, L. V. Yashina, H. Ebert, M. Z. Hasan, O. Rader, Photoemission of Bi_2Se_3 with circularly polarized light: Probe of spin polarization or means for spin manipulation? *Phys. Rev. X* **4**, 011046 (2014).
48. E. Plum, V. A. Fedotov, N. I. Zheludev, Optical activity in extrinsically chiral metamaterial. *Appl. Phys. Lett.* **93**, 191911 (2008).
49. H. N. S. Krishnamoorthy, G. Adamo, J. Yin, V. Savinov, N. I. Zheludev, C. Soci, Infrared dielectric metamaterials from high refractive index chalcogenides. *Nat. Commun.* **11**, 1692 (2020).
50. J.-Y. Ou, J.-K. So, G. Adamo, A. Sulaev, L. Wang, N. I. Zheludev, Ultraviolet and visible range plasmonics in the topological insulator $Bi_{1.5}Sb_{0.5}Te_{1.8}Se_{1.2}$. *Nat. Commun.* **5**, 5139 (2014).
51. S. Y. Matsushita, K. K. Huynh, H. Yoshino, N. H. Tu, Y. Tanabe, K. Tanigaki, Thermoelectric properties of 3D topological insulator: Direct observation of topological surface and its gap opened states. *Phys. Rev. Mater.* **1**, 054202 (2017).
52. O. Madelung, *Semiconductors Data Handbook* (Springer, 2004), pp. 691.

Acknowledgments: We would like to acknowledge J. Song for insightful discussions on fundamental processes underlying HDPC in Dirac materials; A. Dubrovkin, G. Yuan, and S. Aljunid for technical consultations; and W. Lan for providing the BSTS crystal. **Funding:** This research was supported by the Singapore Ministry of Education [grant no. MOE2016-T3-1-006 (S)], the UK Engineering and Physical Sciences Research Council (grant no.: EP/M009122/1) and the Singapore National Research Foundation, Prime Minister's Office, under its Quantum Engineering Programme (grant no.: QEP-P1). M.E. acknowledges the 100 Foreign Talents Project in Jiangsu Province (JSA2016003) and the National Natural Science Foundation of China (NSFC 11774170) for travel support. **Author contributions:** C.S., M.E., and G.A. conceived the original idea. X.S. developed experimental setup with initial assistance from M.E. and performed all HDPC measurements. G.A. and X.S. developed the device fabrication process (G.A. fabricated the metamaterials and X.S. fabricated the devices). G.A. performed the electromagnetic simulations. H.N.S.K. did ellipsometric measurements and extracted the optical constants. X.S., G.A., and C.S analyzed the data and drafted the manuscript. All authors contributed to the discussion and revision of the manuscript. C.S. and N.I.Z. supervised the work. **Competing interests:** The authors declare that they have no competing interests. **Data and materials availability:** All data needed to evaluate the conclusions in the paper are present in the paper and/or the Supplementary Materials. The data that support the findings of this study are openly available in NTU research data repository DR-NTU (Data) at https://doi.org/10.21979/N9/U9UXXV. Additional data related to this paper may be requested from the authors.

Submitted 31 August 2020
Accepted 12 February 2021
Published 2 April 2021
10.1126/sciadv.abe5748

Citation: X. Sun, G. Adamo, M. Eginligil, H. N. S. Krishnamoorthy, N. I. Zheludev, C. Soci, Topological insulator metamaterial with giant circular photogalvanic effect. *Sci. Adv.* **7**, eabe5748 (2021).

Topological insulator metamaterial with giant circular photogalvanic effect

X. Sun, G. Adamo, M. Eginligil, H. N. S. Krishnamoorthy, N. I. Zheludev, and C. Soci

Sci. Adv., **7** (14), eabe5748.
DOI: 10.1126/sciadv.abe5748